ISSN: 1692-7257 - Volume 2 – Number 48 - 2026

RCTA
Revista Colombiana de Tecnologías de Avanzada
UNIPAMPLONA

Digital Object Identifier: 10.24054/rcta.v2i48.4560

Electrodeposition and morphological characterization of NiS_x coatings on nickel foam

Electrodeposición y caracterización morfológica de capas de NiS_x sobre espuma de níquel

MSc. Claudia Patricia Parra Medina[1,2], PhD. Edwin García Quintero[3]
MSc. Héctor Darío Sánchez Londoño[4]

[1] ***Universidad de Antioquia,*** *Facultad de Ingenierías, Programa de Doctorado en Ingeniería de Materiales, Medellín, Antioquia, Colombia.*
[2] ***Universidad Militar Nueva Granada,*** *Facultad de Ingenierías, Programa de Ingeniería en Mecatrónica, Bogotá D.C, Colombia.*
[3] ***Universidad de Antioquia,*** *Facultad de Ingenierías, Programa de Ingeniería Eléctrica, Medellín, Antioquia, Colombia.*
[4] ***Universidad de Antioquia,*** *Facultad de Ingenierías, Programa de Ingeniería de Materiales, Medellín, Antioquia, Colombia.*

Correspondence: *claudia.parra@unimilitar.edu.co*

Received: *february 17, 2026.* ***Accepted:*** *june 23, 2026.* ***Published:*** *july 07, 2026.*

How to cite: *C. P. Parra Medina, E. García Quintero, and H. D. Sánchez Londoño, "Electrodeposition and morphological characterization of NiS_x coatings on nickel foam", RCTA, vol. 2, n.º. 48, pp. 79–88, jul. 2026. Recovered from https://ojs.unipamplona.edu.co/index.php/rcta/article/view/4560*

Abstract: This work evaluates two electrodeposition routes for obtaining nickel-sulfur (NiS_x) coatings on nickel foam substrates. The objective was to compare the effect of deposition conditions on surface morphology, coating thickness, and elemental Ni/S ratio of the resulting films. The first route was developed using potentiodynamic electrodeposition at a scan rate of 5 mV s^{-1}, between -0.54 and -1.44 V, for eight cycles. The second route was carried out using two current density steps, applying 10 mA cm^{-2} for 90 min and 100 mA cm^{-2} for 75 min. The resulting coatings were characterized by field emission scanning electron microscopy (FESEM) and energy-dispersive X-ray spectroscopy (EDX). Synthesis 1 produced a relatively uniform film with a fine granular morphology and lamellar growth associated with deposition cycles, with an average thickness of approximately 720 nm and a Ni/S atomic ratio close to 1:1. Synthesis 2 generated a cauliflower-like surface morphology, with a greater average thickness of approximately 700 nm and a Ni/S atomic ratio close to 2.5:1. These results show that the electrodeposition conditions significantly modify the microstructure, growth mode, and elemental composition of NiS_x coatings on nickel foam. This study provides useful experimental information for the design and optimization of nickel-sulfur films obtained by electrodeposition.

Keywords: electrodeposition; nickel sulfide; nickel foam; NiS_x coatings; FESEM; EDX; surface morphology; Ni/S ratio.

Resumen: En este trabajo se evaluaron dos rutas de electrodeposición para obtener recubrimientos de sulfuro de níquel, NiS_x, sobre sustratos de espuma de níquel. El objetivo fue comparar el efecto de las condiciones de deposición sobre la morfología superficial, el espesor del recubrimiento y la relación elemental Ni/S de las películas obtenidas. La primera ruta se desarrolló mediante electrodeposición potenciodinámica a una velocidad de

barrido de 5 mV s^{-1}, entre -0.54 y -1.44 V, durante ocho ciclos. La segunda ruta se realizó mediante dos escalones de densidad de corriente, aplicando 10 mA cm^{-2} durante 90 min y 100 mA cm^{-2} durante 75 min. Los recubrimientos obtenidos fueron caracterizados mediante microscopía electrónica de barrido por emisión de campo, FESEM, y espectroscopía de energía dispersiva de rayos X, EDX. La síntesis 1 produjo una película relativamente uniforme, con morfología granular fina y crecimiento laminar asociado a los ciclos de deposición, con un espesor promedio aproximado de 720 nm y una relación atómica Ni/S cercana a 1:1. La síntesis 2 generó una morfología superficial tipo coliflor, con mayor espesor promedio aproximado de 700 nm y una relación atómica Ni/S cercana a 2.5:1. Estos resultados muestran que las condiciones de electrodeposición modifican de manera significativa la microestructura, el modo de crecimiento y la composición elemental de los recubrimientos NiS_x sobre espuma de níquel. El estudio aporta información experimental útil para el diseño y optimización de películas de sulfuro de níquel obtenidas por electrodeposición.

Palabras clave: electrodeposición, sulfuro de níquel; espuma de níquel; recubrimientos NiS_x; FESEM; EDX; morfología superficial; relación Ni/S.

1. INTRODUCTION

Hydrogen production through water electrolysis has become a promising alternative for the development of sustainable energy technologies, particularly when coupled with electricity generated from renewable energy sources [1], [11]. However, the implementation of these systems still faces challenges related to the cost, availability, activity, and stability of the materials used as electrodes, especially under demanding operating conditions or in electrolytes containing aggressive species [1], [4], [11], [16], [21], [24], [28].

Water electrolysis involves two main half-reactions: the hydrogen evolution reaction (HER) and the oxygen evolution reaction (OER). Among them, the OER is generally considered the kinetically limiting process because of its multielectron reaction mechanism and the participation of oxygen-containing intermediates adsorbed on the electrode surface [5]–[8]. Consequently, numerous families of transition metal-based materials, including oxides, hydroxides, oxyhydroxides, phosphides, sulfides, selenides, and multicomponent heterostructures, have been extensively investigated as alternatives to noble-metal-based electrocatalysts [5], [9], [10], [12], [19], [29], [31].

Nickel-based materials, in particular, have attracted considerable attention owing to their relative abundance, high electrical conductivity, compatibility with metallic substrates, and ability to form active or precursor phases through electrochemical routes. Systems such as NiFe, NiFe-LDH, NiS_x, $NiS–NiS_2$, and related heterostructures have been reported as promising materials for electrochemical applications, mainly because of the possibility of tailoring their morphology, composition, and interfacial properties with the substrate [3], [4], [15], [18], [20], [21], [24], [29], [30].

Operation in saline media or seawater electrolysis introduces additional challenges due to the presence of chloride ions, competition between anodic reactions, possible formation of chlorinated species, and corrosion or surface degradation phenomena affecting the electrode [1], [4], [11], [16], [21], [24], [28]. These considerations justify the growing interest in developing conductive substrates coated with functional materials capable of modifying the electrode surface. Nevertheless, assigning HER activity, OER activity, selectivity, or electrochemical stability requires specific characterization techniques, including voltammetry, polarization curves, electrochemical impedance spectroscopy, stability tests, or product quantification. Therefore, in the present work these previous studies are used solely as technological background rather than as evidence of the electrocatalytic performance of the synthesized coatings.

Nickel foam is an attractive three-dimensional substrate for the growth of functional coatings because of its porous architecture, high electrical conductivity, and large available surface area for nucleation of deposited materials. These characteristics have promoted its use as a support for transition metal oxides, hydroxides, phosphides, sulfides, and heterostructures [2], [4], [15], [17],

[20], [25], [30]. However, obtaining reproducible coatings on this type of substrate requires understanding how synthesis conditions influence the morphology, thickness, continuity, and elemental composition of the deposited layer.

Among the available synthesis routes, electrodeposition offers significant advantages for fabricating coatings on conductive substrates because it enables precise control of parameters such as the applied potential, current density, scan rate, deposition time, number of cycles, and electrolyte composition [2], [18], [34], [35]. These parameters strongly affect nucleation, growth, coalescence, and film densification, thereby modifying the surface roughness, thickness, adhesion, growth mechanism, and elemental composition of the resulting coatings. Consequently, electrodeposition is not only an effective fabrication technique for functional materials but also a valuable approach for investigating the relationship between synthesis conditions and the microstructure of deposited films.

Nickel sulfides NiS_x belong to the family of transition metal chalcogenides and may exhibit different compositions, morphologies, and Ni/S atomic ratios depending on the synthesis method employed. Materials such as NiS, NiS_2, Ni_3S_2, and related nickel sulfide heterostructures have been reported, some directly supported on nickel foam or combined with other transition metal phases [3], [4], [17], [20], [24], [26], [30]. Likewise, other chalcogenides and nanostructured materials, including MoS_2, WSe_2, and hybrid systems, have been investigated in various electrochemical applications, highlighting the widespread interest in controlling the morphology and composition of this class of materials [25] and [27].

However, the identification of specific nickel sulfide phases requires complementary structural characterization techniques such as X-ray diffraction (XRD). Therefore, analyses based solely on field-emission scanning electron microscopy (FESEM) and energy-dispersive X-ray spectroscopy (EDX) should be interpreted as morphological and compositional evidence rather than as definitive crystallographic confirmation of a particular phase. This distinction is important because the Ni/S elemental ratio determined by EDX may suggest compositions compatible with specific nickel sulfide phases but cannot independently confirm the crystal structure of the deposited coating.

The literature also demonstrates that the morphological and compositional properties of nickel-based materials strongly depend on the synthesis route. Strategies involving electrodeposition, heterostructure formation, interfacial engineering, and three-dimensional nanoarchitectures have been developed to tailor the surface properties of nickel-supported electrodes [2], [3], [15], [18], [20], [29], [30], [34], [35]. Nevertheless, before discussing the functional performance of these materials, it is essential to establish the fundamental characteristics of the deposited films, including coating uniformity, thickness, growth mechanism, surface morphology, and elemental composition.

Previous studies related to electrolysis, OER catalysts, and electrode modification have reported multiple strategies for improving catalytic activity and stability through the incorporation of oxides, hydroxides, oxyhydroxides, phosphides, sulfides, interfacial layers, and hierarchical structures [5], [9], [10], [13], [18], [21], [22], [29], [31]. Additional studies have focused on the development of seawater electrolysis anodes and nanostructured materials derived from reduced graphene oxide or metallic nanoparticles [32], [33]. These investigations provide a general framework highlighting the importance of controlling coating microstructure; however, the scope of the present study is restricted to the morphological and compositional characterization of electrodeposited NiS_x films.

Despite the considerable progress achieved in nickel-based materials and transition metal chalcogenides, additional experimental evidence is still required to clarify how different electrodeposition conditions influence the surface morphology, cross-sectional growth, thickness, and Ni/S elemental ratio of NiS_x coatings directly deposited onto nickel foam. This information is particularly valuable because the microstructure of the coating constitutes a prerequisite for subsequent functional evaluation and provides fundamental criteria for optimizing synthesis conditions before assigning specific electrochemical properties.

The research gap addressed in this work consists of comparing two electrodeposition routes for producing NiS_x coatings on nickel foam using the same morphological and compositional characterization approach. The novelty of this study lies in the comparison between a potentiodynamic cyclic electrodeposition route and a two-step current-density electrodeposition route, evaluating

how these deposition conditions influence the surface morphology, cross-sectional growth mechanism, coating thickness, and Ni/S elemental ratio of the resulting films.

Accordingly, the objective of this work was to synthesize nickel sulfide NiS_x coatings on nickel foam by means of two different electrodeposition routes and to compare the influence of deposition conditions on coating morphology, thickness, cross-sectional growth, and elemental composition. Characterization was carried out using FESEM and EDX. The main contribution of this manuscript is to provide experimental evidence on the relationship between electrodeposition conditions, coating microstructure, and Ni/S elemental ratio in NiS_x films, thereby establishing a basis for future structural and electrochemical investigations.

2. EXPERIMENTAL METHODS

Two electrodeposition routes were investigated to obtain nickel sulfide NiS_x coatings on nickel foam substrates. The objective of this experimental study was to compare the effect of the deposition conditions on the surface morphology, cross-sectional growth, coating thickness, and elemental composition of the resulting films. The nickel foam used as the substrate measured 1 cm × 1 cm and had an areal density of 420 g m^{-2}. Table 1 summarizes the reagents, concentrations, and electrodeposition conditions employed for Synthesis 1 and Synthesis 2.

***Tabla 1**: Reagents and electrodeposition conditions used for each synthesis route.*

Synthesis No.	Synthesis No.	Synthesis No.	Synthesis No.
Synthesis 1	$Ni(NO_3)_2$	0.5 M	Scan rate = 5 mV s^{-1}, with V0 = -0.54 V and Vf = -1.44 V. Eight cycles were performed.
	$Na_2S_2O_3$	0.1M	
Synthesis 2	NaH_2PO_2	0.2M	Current density 1 = 10 mA cm^{-2} for 90 min. Current density 2 = 100 mA cm^{-2} for 75 min.
	$NiCl_2$	0.05M	
	$CS(NH_2)_2$	0.1 M	
	NH_4F	0.15M	

***Source:** Authors.*

The electrodeposition processes for Synthesis 1 and Synthesis 2 were carried out using a two-electrode electrochemical cell, with nickel foam serving as the working electrode and SAE 316L stainless steel as the counter electrode, as illustrated in Fig. 1a. Since a two-electrode configuration was employed, the reported values correspond to the voltage applied between the working and counter electrodes rather than to potentials measured with respect to a reference electrode.

Prior to electrodeposition, the nickel foam substrate was cleaned by immersing the bare nickel foam in 1.0 M HCl for 20 min under ultrasonic agitation. The substrate was subsequently rinsed thoroughly with ethanol and deionized water and allowed to dry at room temperature. The cleaned nickel foam (1 cm × 1 cm), with an exposed geometric area of 1 cm^2, was then immersed in the electrolyte and used as the working electrode.

For each synthesis route, the electrolyte was prepared according to the composition listed in Table 1 and magnetically stirred for approximately 25 min at room temperature (22 ± 2 °C). Synthesis 1 was performed using a programmable DC power supply operating in potentiodynamic mode at a scan rate of 5 mV s^{-1} for eight deposition cycles, with the applied voltage swept from −0.54 V to −1.44 V.

After electrodeposition, the working electrodes were rinsed with deionized water and dried at room temperature. The average mass loading of the deposited film was approximately 1.5 mg cm^{-2}, calculated from the difference in mass of the nickel foam before and after electrodeposition. Synthesis 2 was carried out using the same power supply by applying two consecutive current-density steps: 10 mA cm^{-2} for 90 min followed by 100 mA cm^{-2} for 75 min, as shown in Fig. 1b. After electrodeposition, the working electrodes were again rinsed with deionized water and dried at room temperature.

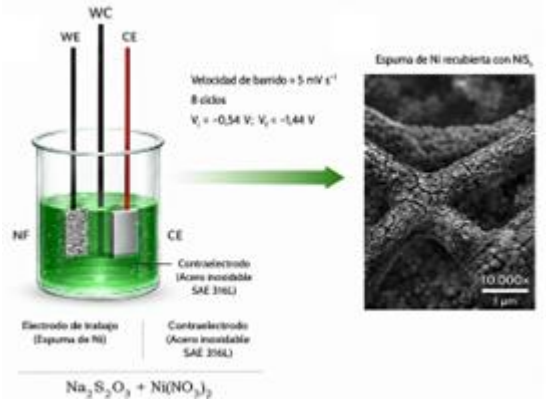

(a) Síntesis 1

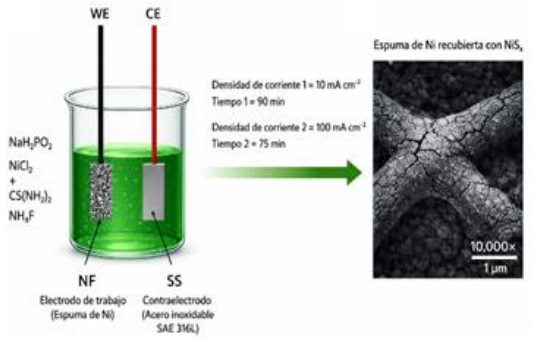

(b) Síntesis 2

Fig. 1. *Schematic illustration of the electrodeposition process: (a) Synthesis 1 and (b) Synthesis 2.* ***Source:*** *Authors.*

The electrodeposition process was repeated 22 times for each synthesis route, yielding 22 specimens for each experimental condition. From this set, representative samples were selected for FESEM–EDX characterization based on the macroscopic integrity of the coating, the absence of visible delamination, and surface continuity. Coating thickness and structural feature size were measured at different locations on the available micrographs to ensure representative characterization of the deposited films.

3. RESULTS AND DISCUSSION

Field-emission scanning electron microscopy (FESEM) and energy-dispersive X-ray spectroscopy (EDX) were employed to characterize the surface morphology, cross-sectional microstructure, and semiquantitative elemental composition of the electrodeposited NiS_x films.

Figure 2 presents the morphological characterization of the coating obtained by Synthesis 1. Figure 2a shows the nickel foam substrate coated with NiS_x The micrograph was acquired using an accelerating voltage of 20.00 kV, a magnification of 200×, and a probe current of 1.6 nA.

Figure 2b shows the NiS_x coating deposited on the nickel foam substrate, acquired at an accelerating voltage of 20.00 kV, a magnification of 1000×, and a probe current of 1.6 nA. The presence of cracks and fractured regions made it possible to observe the cross section of the coating and estimate its thickness. Figure 2c shows the surface morphology of the coating, acquired at an accelerating voltage of 5.00 kV, a magnification of 20,000×, and a probe current of 0.2 nA. The surface is composed of rounded fine-grained nanostructures with an average diameter of approximately 180 nm.

Figure 2d presents a higher-magnification image of the fractured region of the NiS_x coating, acquired at an accelerating voltage of 5.00 kV, a magnification of 30,000×, and a probe current of 25 pA. Based on this micrograph, the average coating thickness was estimated to be approximately 720 nm.

The cross-sectional micrograph reveals a lamellar growth pattern associated with the electrodeposition cycles. The presence of eight distinct sublayers is consistent with the eight deposition cycles applied during Synthesis 1. Figure 3 illustrates the lamellar growth of the coating and the formation of these sublayers resulting from the successive electrodeposition cycles.

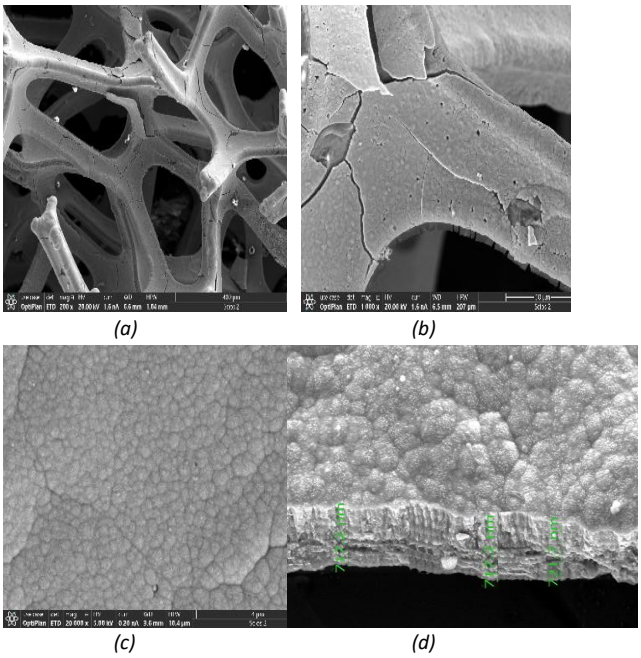

(a) *(b)*

(c) *(d)*

Fig. 2*. FESEM characterization of the coating obtained by Synthesis 1. (a) Nickel foam coated with NiS_x; (b) NiS_x coating; (c) Surface morphology of the NiS_x coating; (d) Cross-sectional view showing the coating thickness.* ***Source:*** *Authors.*

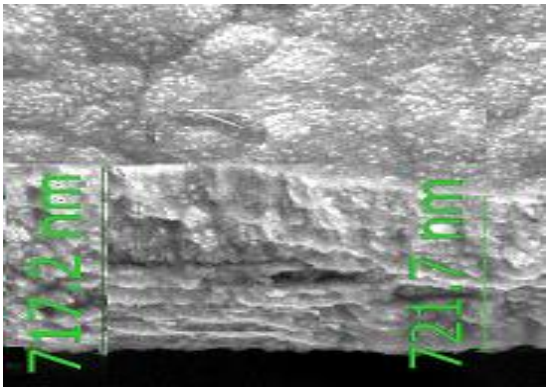

Fig. 3. *Cross-sectional view of the NiS_x coating obtained by Synthesis 1.* ***Source:*** *Authors.*

EDX microanalysis was performed on the coating obtained by Synthesis 1, as shown in Fig. 4. The analysis was carried out in two representative regions: one located in the cross section of the lamellar coating and the other on the surface of the deposited film.

Figure 4a shows the locations selected for the EDX analysis on the surface of the coating obtained by Synthesis 1, whereas Fig. 4b presents the elemental composition results of the coating.

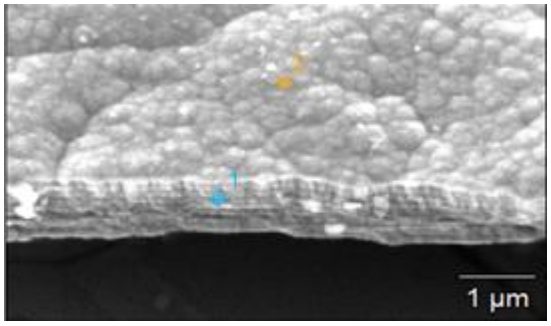

(a)

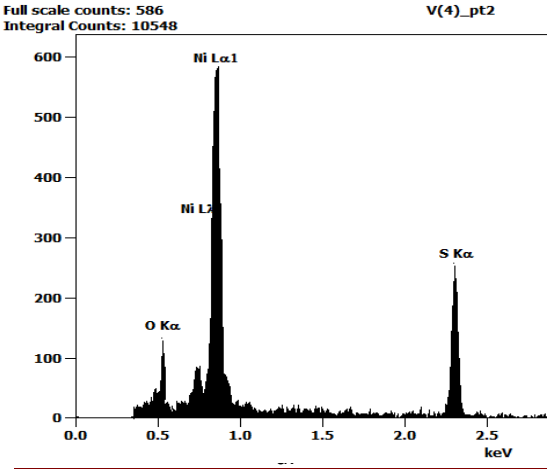

Element	Weight %	Weight % Error	Atom %	Atom % Error
O	1.901	±0.568	4.870	±1.414
S	28.995	±0.684	48.897	±4.650
Ni	69.104	±1.399	45.892	±2.962
Total	100.000		100.000	

(b)

Fig. 4. *EDX microanalysis of the coating obtained by Synthesis 1. (a) Locations selected for EDX analysis on the electrodeposited surface. (b) Elemental composition of the coating.* ***Source:*** *Authors.*

The semiquantitative analysis revealed an atomic Ni/S ratio close to 1:1, suggesting a composition compatible with a NiS_x nickel sulfide coating. However, this assignment should be regarded as approximate because EDX allows the identification and estimation of the local elemental composition but does not provide definitive confirmation of the crystalline phase of the material. Therefore, the specific identification of nickel sulfide phases would require complementary structural characterization techniques such as X-ray diffraction (XRD) [17], [20], [25], [30].

Figure 5 presents the morphological characterization of the coating obtained by Synthesis 2. Figure 5a shows the nickel foam coated with NiS_x. The micrograph was acquired using an accelerating voltage of 20.00 kV, a magnification of 200×, and a probe current of 1.6 nA.

Figure 5b shows the NiS_x coating deposited on the nickel foam substrate. The micrograph was acquired using an accelerating voltage of 20.00 kV, a magnification of 1000×, and a probe current of 1.6 nA. The image reveals a relatively continuous coating on the substrate, with the presence of cracked regions that allowed the cross section of the coating to be observed and its thickness to be estimated.

Figure 5c presents the surface morphology of the coating, acquired at an accelerating voltage of 5.00 kV, a magnification of 20,000×, and a probe current of 0.2 nA. The surface exhibits a heterogeneous morphology associated with the growth of granular structures on the electrodeposited layer. Figure 5d shows a higher-magnification image of a fractured region of the NiS_x coating, acquired at an accelerating voltage of 5.00 kV, a magnification of 30,000×, and a probe current of 25 pA. Synthesis 2 produced a cauliflower-like surface morphology with an average coating thickness of approximately 880 nm and granular substructures measuring approximately 700 nm.

In addition, Fig. 5c provides a closer view of the cauliflower-like structures formed during the electrodeposition process. This micrograph was acquired at an accelerating voltage of 5.00 kV and a magnification of 25,000×. The cauliflower-like structures exhibited an average diameter of approximately 3 µm.

Similarly, Fig. 6a reveals the granular substructures that constitute these cauliflower-like morphologies, with average sizes of approximately 700 nm. This distinction makes it possible to differentiate between the overall dimensions of the cauliflower-like structures and the size of the individual granular units that compose them. Figure 6b shows the cross section of the coating obtained by Synthesis 2. The micrograph reveals that two distinct sublayers with different morphologies were formed during the two

electrodeposition current-density steps on the nickel foam substrate. During the first step, performed at a current density of 10 mA cm^{-2}, a predominantly columnar sublayer was formed. During the second step, carried out at 100 mA cm^{-2}, a coarser-grained sublayer developed, corresponding to the cauliflower-like morphology observed on the coating surface. Although deposited for a shorter period, the sublayer formed during the second current-density step exhibited a greater thickness than that produced during the first step.

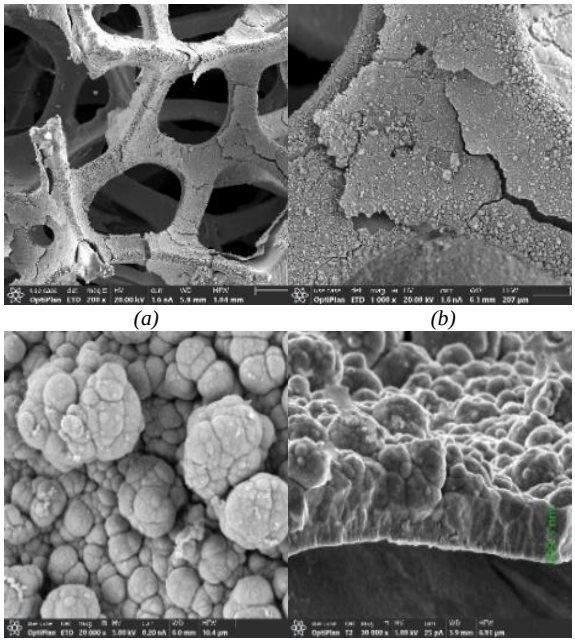

(a) *(b)*

(c) *(d)*

***Fig. 5**. FESEM characterization of the NiS_x coating obtained by Synthesis 2. (a) NiS_x-coated nickel foam. (b) NiS_x coating. (c) Surface morphology of the NiS_x coating. (d) Cross-sectional view showing the coating thickness. **Source:** Authors.*

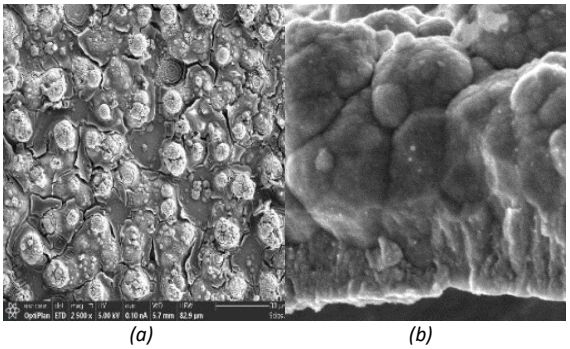

(a) *(b)*

***Fig. 6**. Cross-sectional FESEM image of the NiS_x coating obtained by Synthesis 2. **Source:** Authors.*

Finally, EDX microanalysis was performed on the coating obtained by Synthesis 2, as shown in Fig. 7. The analysis was carried out on representative regions of the film, including one located in the cross section of the sublayers formed during electrodeposition and another on the coating surface. Figure 7a shows the locations selected for the EDX analysis, whereas Fig. 7b presents the corresponding elemental composition results.

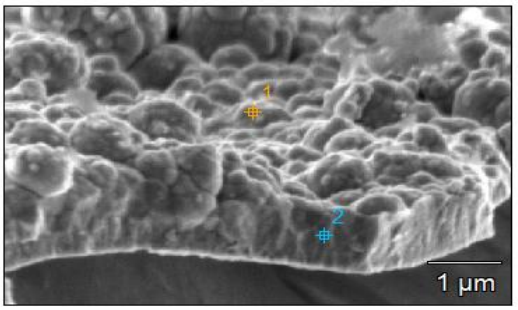

(a)

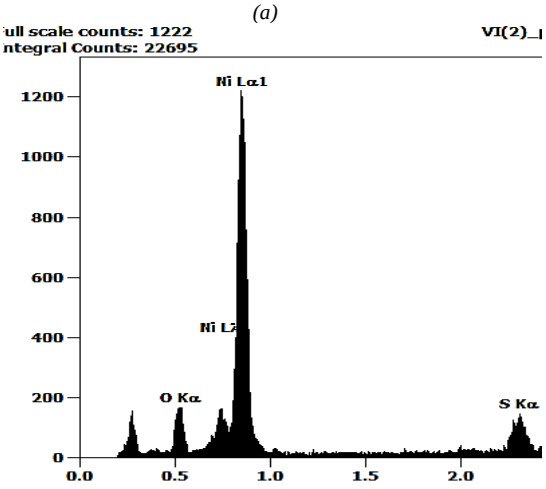

Element	Weight %	Weight % Error	Atom %	Atom % Error
O	3.789	±0.284	11.165	±2.511
S	17.338	±0.703	25.497	±3.102
Ni	78.873	±0.937	63.338	±2.257
Total	100.000		100.000	

(b)

***Fig. 7.** EDX microanalysis of the NiS_x coating obtained by Synthesis 2. (a) Selected locations for EDX analysis on the electrodeposited surface. (b) Elemental composition of the coating. **Source:** Authors.*

The semiquantitative analysis revealed an atomic Ni/S ratio of approximately 2.5:1, indicating that the coating obtained by Synthesis 2 was enriched in nickel compared with that produced by Synthesis 1. However, this ratio should be interpreted as a local compositional estimate because EDX alone cannot confirm the crystalline phase of the nickel sulfide formed. Definitive phase identification would require complementary structural characterization techniques such as X-ray diffraction (XRD).

A comparison of the two electrodeposition routes shows that the deposition conditions simultaneously

affected the coating morphology, thickness, and Ni/S ratio. Synthesis 1 produced a lamellar film with an average thickness of approximately 720 nm and an atomic Ni/S ratio close to 1:1. In contrast, Synthesis 2 generated a cauliflower-like morphology with an average coating thickness of approximately 880 nm and an atomic Ni/S ratio of approximately 2.5:1. These results indicate that the higher current density employed during the second deposition route promoted faster film growth and produced a nickel-rich coating. This behavior may be associated with differences in the reduction kinetics, mass transport, and local availability of sulfur-containing species during the electrodeposition process.

The oxygen detected by EDX should be interpreted as a surface-related signal associated with the chemical state of the coating and its exposure to the surrounding environment rather than as direct evidence of a specific crystalline phase. Synthesis 1 exhibited an oxygen content of 4.870 at.%, whereas Synthesis 2 showed an increased oxygen content of 11.165 at.%. This difference may be attributed to the greater exposed surface area of the cauliflower-like morphology produced during Synthesis 2, which may favor the adsorption of oxygen-containing species, moisture, or surface residues after washing and drying. In addition, the presence of oxygen may be associated with surface oxidation of nickel or nickel sulfides during drying and storage under ambient conditions, as well as with the possible formation of hydroxide or oxyhydroxide species on the coating surface.

It should also be considered that EDX is a semiquantitative technique and that its results depend on the selected analysis region. Therefore, the reported elemental compositions should be interpreted as local compositional information rather than as representative of the entire coating. Consequently, the accurate identification of oxide, hydroxide, or oxyhydroxide phases would require complementary characterization techniques such as XRD, XPS, or Raman spectroscopy.

4. CONCLUSIONS

Nickel sulfide (NiS_x) coatings were successfully deposited onto nickel foam substrates using two different electrodeposition routes. Synthesis 1, based on cyclic potentiodynamic electrodeposition, produced a coating with a fine-grained surface morphology composed of rounded features. Cross-sectional observations revealed a lamellar growth pattern, with distinct sublayers corresponding to the successive electrodeposition cycles.

Synthesis 2, carried out using a two-step current-density electrodeposition process, produced a coating with a cauliflower-like surface morphology. Cross-sectional analysis revealed differences between the sublayers formed during each deposition step. During the first step, performed at 10 mA cm^{-2}, a predominantly columnar sublayer was formed, whereas the second step, conducted at 100 mA cm^{-2}, generated a coarser-grained sublayer associated with the cauliflower-like morphology. These findings indicate that increasing the current density significantly influenced both the morphology and thickness of the deposited coating.

EDX microanalysis confirmed the presence of nickel and sulfur in the coatings produced by both synthesis routes. Synthesis 1 exhibited an atomic Ni/S ratio close to 1:1, whereas Synthesis 2 showed an approximate Ni/S ratio of 2.5:1, indicating compositional differences associated with the electrodeposition conditions. However, because EDX provides only semiquantitative elemental information, the identification of specific crystalline nickel sulfide phases requires complementary structural characterization techniques such as X-ray diffraction (XRD).

Overall, the results demonstrate that the electrodeposition conditions directly affect the surface morphology, cross-sectional growth, coating thickness, and Ni/S elemental ratio of NiS_x films deposited on nickel foam. This study provides valuable experimental information for the design and optimization of nickel sulfide coatings on conductive porous substrates, serving as a foundation for future structural and electrochemical investigations.

A limitation of the present study is that the characterization was restricted to morphological and compositional analyses using FESEM and EDX. Consequently, neither the specific crystalline phases of the coatings nor their electrochemical performance could be confirmed. Future work should complement these findings with structural characterization techniques such as XRD, XPS, and Raman spectroscopy, as well as electrochemical analyses including voltammetry, electrochemical impedance spectroscopy (EIS), polarization curves, and stability tests.

Funding: Claudia Patricia Parra Medina's doctoral studies were funded by the University of Antioquia through the UdeA Doctoral Scholarship Fund (2022), from which this work was derived.

Acknowledgments: The authors gratefully acknowledge the University of Antioquia for supporting Claudia Patricia Parra Medina's doctoral studies, within the framework of which this research was conducted. The authors also thank the Universidad Militar Nueva Granada (UMNG) for providing the academic environment that facilitated the partial preparation of this manuscript during the author's academic appointment at the institution.

REFERENCES

[1] J. Mohammed-Ibrahim and H. Moussab, "Recent advances on hydrogen production through seawater electrolysis," *Mater. Sci. Energy Technol.*, vol. 3, pp. 780–807, Jan. 2020, doi: 10.1016/j.mset.2020.09.005.

[2] R. Li *et al.*, "Electrodeposition: Synthesis of advanced transition metal-based catalyst for hydrogen production via electrolysis of water," *Journal of Energy Chemistry*, vol. 57. Elsevier B.V., pp. 547–566, Jun. 01, 2021. doi: 10.1016/j.jechem.2020.08.040.

[3] Y. Yang *et al.*, "The in-situ construction of NiFe sulfide with nanoarray structure on nickel foam as efficient bifunctional electrocatalysts for overall water splitting," *J. Alloys Compd.*, vol. 874, Sep. 2021, doi: 10.1016/j.jallcom.2021.159874.

[4] H. Y. Wang *et al.*, "Synergistically enhanced activity and stability of bifunctional nickel phosphide/sulfide heterointerface electrodes for direct alkaline seawater electrolysis," *J. Energy Chem.*, vol. 75, pp. 66–73, Dec. 2022, doi: 10.1016/j.jechem.2022.08.019.

[5] A. Higareda, D. L. Hernández-Arellano, L. C. Ordoñez, R. Barbosa, and N. Alonso-Vante, "Advanced Electrocatalysts for the Oxygen Evolution Reaction: From Single- to Multielement Materials," *Catalysts*, vol. 13, no. 10. Multidisciplinary Digital Publishing Institute (MDPI), Oct. 01, 2023. doi: 10.3390/catal13101346.

[6] T. Reier, H. N. Nong, D. Teschner, R. Schlögl, and P. Strasser, "Electrocatalytic Oxygen Evolution Reaction in Acidic Environments – Reaction Mechanisms and Catalysts," *Advanced Energy Materials*, vol. 7, no. 1. Wiley-VCH Verlag, Jan. 11, 2017. doi: 10.1002/aenm.201601275.

[7] Z. Yan, H. Liu, Z. Hao, M. Yu, X. Chen, and J. Chen, "Electrodeposition of (hydro)oxides for an oxygen evolution electrode," *Chemical Science*, vol. 11, no. 39. Royal Society of Chemistry, pp. 10614–10625, Oct. 21, 2020. doi: 10.1039/d0sc01532f.

[8] J. Rossmeisl, A. Logadottir, and J. K. Nørskov, "Electrolysis of water on (oxidized) metal surfaces," *Chem. Phys.*, vol. 319, no. 1–3, pp. 178–184, Dec. 2005, doi: 10.1016/j.chemphys.2005.05.038.

[9] F. Song *et al.*, "Transition Metal Oxides as Electrocatalysts for the Oxygen Evolution Reaction in Alkaline Solutions: An Application-Inspired Renaissance," *J. Am. Chem. Soc.*, vol. 140, no. 25, pp. 7748–7759, Jun. 2018, doi: 10.1021/jacs.8b04546.

[10] J. W. D. Ng *et al.*, "Gold-supported cerium-doped NiOx catalysts for water oxidation," *Nat. Energy*, vol. 1, no. 5, p. 16053, Apr. 2016, doi: 10.1038/nenergy.2016.53.

[11] S. Jiang *et al.*, "Recent Advances in Seawater Electrolysis," *Catalysts*, vol. 12, no. 2. MDPI, Feb. 01, 2022. doi: 10.3390/catal12020123.

[12] L. An *et al.*, "Recent Development of Oxygen Evolution Electrocatalysts in Acidic Environment," *Adv. Mater.*, vol. 33, no. 20, May 2021, doi: 10.1002/adma.202006328.

[13] B. Zhang *et al.*, "Homogeneously dispersed multimetal oxygen-evolving catalysts." [Online]. Available: https://www.science.org

[14] M. S. Burke, M. G. Kast, L. Trotochaud, A. M. Smith, and S. W. Boettcher, "Cobalt-Iron (Oxy)hydroxide Oxygen Evolution Electrocatalysts: The Role of Structure and Composition on Activity, Stability, and Mechanism," *J. Am. Chem. Soc.*, vol. 137, no. 10, pp. 3638–3648, Mar. 2015, doi: 10.1021/jacs.5b00281.

[15] X. Lu and C. Zhao, "Electrodeposition of hierarchically structured three-dimensional nickel-iron electrodes for efficient oxygen evolution at high current densities," *Nat. Commun.*, vol. 6, Mar. 2015, doi: 10.1038/ncomms7616.

[16] B. Zhang *et al.*, "High Corrosion Resistance of NiFe-Layered Double Hydroxide Catalyst for Stable Seawater Electrolysis Promoted by Phosphate Intercalation," *Small*, vol. 18, no. 45, Nov. 2022, doi: 10.1002/smll.202203852.

[17] Y. Li, T. Dai, Q. Wu, X. Lang, L. Zhao, and Q. Jiang, "Design heterostructure of NiS–NiS2 on NiFe layered double hydroxide with Mo doping for efficient overall water splitting," *Mater. Today Energy*, vol. 23, Jan. 2022, doi: 10.1016/j.mtener.2021.100906.

[18] C. G. Morales-Guio, L. Liardet, and X. Hu, "Oxidatively Electrodeposited Thin-Film Transition Metal (Oxy)hydroxides as Oxygen Evolution Catalysts," *J. Am. Chem. Soc.*, vol. 138, no. 28, pp. 8946–8957, Jul. 2016, doi: 10.1021/jacs.6b05196.

[19] F. Calle-Vallejo, O. A. Díaz-Morales, M. J. Kolb, and M. T. M. Koper, "Why is bulk thermochemistry a good descriptor for the electrocatalytic activity of transition metal oxides?," *ACS Catal.*, vol. 5, no. 2, pp. 869–873, Feb. 2015, doi: 10.1021/cs5016657.

[20] B. Cui *et al.*, "Heterogeneous lamellar-edged Fe-Ni(OH)2/Ni3S2 nanoarray for efficient and stable seawater oxidation," *Nano Res.*, vol. 14, no. 4, pp. 1149–1155, Apr. 2021, doi: 10.1007/s12274-020-3164-3.

[21] A. R. Jadhav *et al.*, "Stable complete seawater electrolysis by using interfacial chloride ion blocking layer on catalyst surface," *J. Mater. Chem. A*, vol. 8, no. 46, pp. 24501–24514, Dec. 2020, doi: 10.1039/d0ta08543j.

[22] F. Dionigi, T. Reier, Z. Pawolek, M. Gliech, and P. Strasser, "Design Criteria, Operating Conditions, and Nickel-Iron Hydroxide Catalyst Materials for Selective Seawater Electrolysis," *ChemSusChem*, vol. 9, no. 9, pp. 962–972, May 2016, doi: 10.1002/cssc.201501581.

[23] S. H. Hsu *et al.*, "An Earth-Abundant Catalyst-Based Seawater Photoelectrolysis System with 17.9% Solar-to-Hydrogen Efficiency," *Adv. Mater.*, vol. 30, no. 18, May 2018, doi: 10.1002/adma.201707261.

[24] Y. Kuang *et al.*, "Solar-driven, highly sustained splitting of seawater into hydrogen and oxygen fuels," *Proc. Natl. Acad. Sci. U. S. A.*, vol. 116, no. 14, pp. 6624–6629, Apr. 2019, doi: 10.1073/pnas.1900556116.

[25] J. Lin *et al.*, "Defect-Rich Heterogeneous MoS2/NiS2 Nanosheets Electrocatalysts for Efficient Overall Water Splitting," *Adv. Sci.*, vol. 6, no. 14, Jul. 2019, doi: 10.1002/advs.201900246.

[26] Y. Fang *et al.*, "Experiments combined with theoretical research on the effect of hydrogen evolution by the nanosheet of NiS–CdS–CN catalyst," *Int. J. Hydrogen Energy*, vol. 47, no. 12, pp. 7724–7737, Feb. 2022, doi: 10.1016/j.ijhydene.2021.12.098.

[27] K. Share, J. Lewis, L. Oakes, R. E. Carter, A. P. Cohn, and C. L. Pint, "Tungsten diselenide (WSe2) as a high capacity, low overpotential conversion electrode for sodium ion batteries," *RSC Adv.*, vol. 5, no. 123, pp. 101262–101267, 2015, doi: 10.1039/c5ra19717a.

[28] Z. Kato, N. Kumagai, K. Asami, and K. Hashimoto, "The Effect of Tungsten Addition to the Intermediate IrO2 Layer of Mn-Mo-O/IrO2/Ti Electrodes on the Performance for Oxygen Evolution in Seawater Electrolysis," *ECS Meet. Abstr.*, vol. MA2005-02, no. 8, pp. 377–377, 2006, doi: 10.1149/ma2005-02/8/377.

[29] D. Zhou *et al.*, "Layered double hydroxide-based electrocatalysts for the oxygen evolution reaction: Identification and tailoring of active sites, and superaerophobic nanoarray electrode assembly," *Chemical Society Reviews*, vol. 50, no. 15. Royal Society of Chemistry, pp. 8790–8817, Aug. 07, 2021. doi: 10.1039/d1cs00186h.

[30] G. Zhang *et al.*, "Design and construction of hierarchical Ni3S2 @V-doped NiMn-LDH heterostructure on rGO/Ni foam as an advanced electrode for battery-supercapacitor hybrid devices," *J. Alloys Compd.*, vol. 896, Mar. 2022, doi: 10.1016/j.jallcom.2021.163125.

[31] W. D. Chemelewski, H. C. Lee, J. F. Lin, A. J. Bard, and C. B. Mullins, "Amorphous FeOOH oxygen evolution reaction catalyst for photoelectrochemical water splitting," *J. Am. Chem. Soc.*, vol. 136, no. 7, pp. 2843–2850, Feb. 2014, doi: 10.1021/ja411835a.

[32] Marisol Soledad Maril Millán, "Desarrollo de un ánodo electrocatalítico para electrólisis de agua de mar," 2022.

[33] Rodríguez Rodríguez Jordi, "Síntesis y Caracterización de Óxido de Grafeno Reducido Funcionalizado con Nanopartículas Metálicas. Aplicación en el Desarrollo de Sensores Amperométricos Basados en Materiales Nanoestructurados," 2020.

[34] C. Wang, Y. Wu, Z. Zhou, J. Wang, S. Pei, and S. Liu, "Electrodeposited amorphous nickel–iron phosphide and sulfide derived films for electrocatalytic oxygen evolution," *Int. J. Hydrogen Energy*, vol. 47, no. 97, pp. 40849–40859, 2022, doi: 10.1016/j.ijhydene.2022.09.200.

[35] M. J. Kenney *et al.*, "An electrodeposition approach to metal/metal oxide heterostructures for active hydrogen evolution catalysts in near-neutral electrolytes," *Nano Res.*, 2019, doi: 10.1007/s12274-019-2379-7.